PROTEINS
STRUCTURE ■ FUNCTION ■ BIOINFORMATICS

Crystal structure of the ω-aminotransferase from *Paracoccus denitrificans* and its phylogenetic relationship with other Class III aminotransferases that have biotechnological potential

Christian Rausch, Alexandra Lerchner, André Schiefner, and Arne Skerra*

Munich Center for integrated Protein Science (CiPSM) and Lehrstuhl für Biologische Chemie, Technische Universität München, Freising-Weihenstephan, Germany

ABSTRACT

Apart from their crucial role in metabolism, pyridoxal 5′-phosphate (PLP)-dependent aminotransferases (ATs) constitute a class of enzymes with increasing application in industrial biotechnology. To provide better insight into the structure-function relationships of ATs with biotechnological potential we performed a fundamental bioinformatics analysis of 330 representative sequences of pro- and eukaryotic Class III ATs using a structure-guided approach. The calculated phylogenetic maximum likelihood tree revealed six distinct clades of which the first segregates with a very high bootstrap value of 92%. Most enzymes in this first clade have been functionally well characterized, whereas knowledge about the natural functions and substrates of enzymes in the other branches is sparse. Notably, in those clades 2-6 members of the peculiar class of ω-ATs prevail, many of which have proven useful for the preparation of chiral amines or artificial amino acids. One representative is the ω-AT from *Paracoccus denitrificans* (PD ω-AT) which catalyzes, for example, the transamination in a novel biocatalytic process for the production of L-homoalanine from L-threonine. To gain structural insight into this important enzyme, its X-ray analysis was carried out at a resolution of 2.6 Å, including the covalently bound PLP as well as 5-aminopentanoate as a putative amino donor substrate. On the basis of this crystal structure in conjunction with our phylogenetic analysis, we have identified a generic set of active site residues of ω-ATs that are associated with a strong preference for aromatic substrates, thus guiding the discovery of novel promising enzymes for the biotechnological production of corresponding chiral amines.

Proteins 2013; 81:774–787.

Key words: active site; chiral amine; fold type I; phylogeny; PLP; substrate specificity; transaminase.

INTRODUCTION

The versatile co-enzyme pyridoxal phosphate (PLP) is well known for its important function in various biocatalytic processes. PLP-dependent biochemical reactions can be classified according to the position of the substrate molecule at which the modification occurs:[1] reactions at the α-position include transamination, decarboxylation, racemization, and elimination or substitution of an electrophilic group whereas those at the β- or γ-position are limited to elimination or substitution reactions.[2]

Those PLP enzymes whose three-dimensional structures are known to date have been classified into five different protein folds.[3] The majority of these enzymes belongs to fold Type I, the so-called "aspartate aminotransferase family," which includes many functionally well-characterized enzymes such as aromatic aminotransferases, glycine acetyltransferase, or prokaryotic ornithine decarboxylase.[2] Representatives of the other four fold types include, for example, tryptophan synthase β subunit (Type II), eukaryotic ornithine decarboxylase (Type III), D-alanine/Class IV aminotransferases (Type IV; here

Additional Supporting Information may be found in the online version of this article.

Abbreviations: AT, aminotransferase; CV ω-AT, ω-AT from *Chromobacterium violaceum*; PD ω-AT, ω-AT from *Paracoccus denitrificans*; PLP, pyridoxal 5′-phosphate; PMP, pyridoxamine phosphate; RMSD, root mean square deviation; SEC, size exclusion chromatography; VF ω-AT, ω-AT from *Vibrio fluvialis*.

Grant sponsor: German Bundesministerium für Bildung und Forschung as part of the Project "Bioxamine" in collaboration with Evonik Industries AG, Marl, Germany
*Correspondence to: Arne Skerra, Lehrstuhl für Biologische Chemie, Technische Universität München, 85350 Freising-Weihenstephan, Germany.
E-mail: skerra@tum.de
Received 27 August 2012; Revised 12 November 2012; Accepted 21 November 2012
Published online 12 December 2012 in Wiley Online Library (wileyonlinelibrary.com).
DOI: 10.1002/prot.24233

PLP is bound in a manner almost opposite to the fold Type I binding site, such that the *re* rather than its *si* face is solvent exposed), and glycogen phosphorylase (Type V).[4,5]

All these enzymes function as homo-dimers or higher-order oligomers, with the active site located at the subunit interface and essential residues contributed by both monomers.[2] Within the PLP-binding sites, these enzymes possess two conserved regions: a lysine residue that forms the Schiff base with PLP and a glycine-rich loop that interacts with the phosphate moiety of the coenzyme.[4] Recently, the B6 database (http://bioinformatics.unipr.it/B6db) has provided a new resource for the identification, classification and comparative analysis of PLP enzymes.[5] This database contains documented catalytic activities dependent on vitamin B6 (PLP) and the corresponding protein families, defined as monophyletic groups of protein sequences possessing the same enzymatic function.

In aminotransferases (ATs), which usually belong to the fold Types I and IV, an amino group from a donor substrate is first transferred to the covalently bound PLP to form pyridoxamine phosphate (PMP), which is followed by transfer to the carbonyl moiety of an acceptor substrate, thus completing the catalytic cycle and regenerating the prosthetic group. Based on common structural characteristics as well as sequence motifs among the fold Type I one can further distinguish 5 AT classes (I–V).[4,6] The ω-AT of *Paracoccus denitrificans* (PD ω-AT; EC 2.6.1.18), which is in the focus of this report, belongs to Class III. Other prominent and well described members of this class show transamination activity towards putrescine (EC 2.6.1.82), acetylornithine (EC 2.6.1.11), ornithine (EC 2.6.1.13), glutamate-1-semialdehyde (EC 5.4.3.8), D-phenyl-glycine (EC 2.6.1.72), diamino-butyrate (EC 2.6.1.62), alanine-glyoxylate (EC 2.6.1.44), 4-amino-butyrate (EC 2.6.1.19), ϵ-lysine (EC 2.6.1.36), β-alanine (EC 2.6.1.18), and taurine (EC 2.6.1.77).[4] With the exception of the putrescine AT, all substrates of these Class III members are amino acids whose transferred amino group is distal to the carboxylate group, hence lending the name "ω-amino (acid) transferases."[7] In fact, ω-ATs constitute the majority of the Class III ATs.

ω-ATs are of particular interest for the biocatalytic preparation of chiral amines, thus facilitating asymmetric syntheses at preparative or even industrial scale.[8] A large number of ω-ATs useful in this regard have been described,[9] offering fast turnover rate, stringent enantioselectivity, and high enzyme stability. The ω-AT with the broadest application spectrum at present originates from *Vibrio fluvialis* (VF ω-AT).[10] Recently, the crystal structure of VF ω-AT has been solved (PDB code: 3NUI; Jang *et al.*, unpublished). Unfortunately, despite the apparently good resolution (2 Å), the available structural model exhibits ill-defined segments and lacks the cofactor PLP, which compromises its value for detailed analysis. The homologous PD ω-AT possesses 94% amino acid sequence identity and was recently characterized in the context of a novel biocatalytic production route for L-homoalanine from L-threonine using a coupled enzymatic reaction with a threonine deaminase.[11] The homologous ω-AT from *Chromobacterium violaceum* (CV ω-AT) also belongs to the Class III ATs and, similarly, shows preference for aromatic substrates.[12] The three-dimensional structure of CV ω-AT, which shares only 38% amino acid sequence identity with the PD ω-AT, was recently published.[13]

In the present study we have subclassified the ATs from Class III using a phylogenetic approach and we describe the crystal structure of the PD ω-AT.

MATERIALS AND METHODS

Identification of Class III AT sequences

To generate an initial phylogenetic tree and a search model for ω-ATs, the amino acid sequence of the Class III PD ω-AT (Uniprot ID A1B956), serving as a relevant representative with biotechnological potential, was compared against the pdb70 database (structures in the PDB having at most 70% sequence identity) using HHpred.[14,15] The 28 resulting homologous three-dimensional structures as well as the sequences of some Class III ATs from a patent[16] were aligned with T-Coffee[17] using the "accurate" (structure-guided) mode. From the resulting structure-guided sequence alignment an initial tree was calculated according to the Maximum Likelihood (ML) method implemented in RAxML.[18] A significant edge with 100% bootstrap support divided the tree into two subtrees corresponding either to "clade 1" or to all other sequences assumed to be ω-ATs, which were subsequently selected for further analysis. To this end, a profile HMM was created from these sequences (called ω-AT-pHMM) using HMMER3.[19]

To search additional suitable representatives of all existing Class III AT sequences in the Uniprot[20] database, the Pfam[6] model for Class III ATs (profile HMM *Aminotran_3*) (PF00202; http://pfam.sanger.ac.uk/family/PF00202) was used to search the UniRef50 sequence database, which covers a reduced set of protein sequences that maximally share 50% mutual identity (http://www.ebi.ac.uk/uniref).

The sequences from this search in UniRef50 and all sequences from the initial tree were united and scored with the ω-AT-pHMM profile. All top-scoring sequences up to the last ω-AT of the initial tree were taken to the next round. Of the remaining UniRef50 sequences assumed to belong to clade 1 only those listed in the SwissProt database[21] were selected (after manual removal of apparently problematic—e.g., "overlong"—sequences). The obtained set of ω-ATs and clade 1 sequences was aligned (structure-guided) and an ML tree was calculated as described above and used to identify or confirm the ω-AT sequences which were selected to build a refined

ω-AT-pHMM profile. After one additional iteration with this pHMM (search in UniRef50 resulting in 756 sequences, selection of sequences, and tree building) the significant division between clade 1 (205 SwissProt sequences) and other ω-ATs (125 UniRef50 sequences) was confirmed. The final set of altogether 330 sequences was realigned using T-Coffee and formatted with Aline.[22]

Cloning of the PD ω-AT gene and protein production

The synthetic coding region for PD ω-AT, optimized for expression in *Escherichia coli*, was amplified from the plasmid pET21a(+)-pCR6 (kindly provided by Evonik Industries, Marl, Germany) via PCR using the primers 5′-GCCAACCAACCGCAAAGCTGGGA-3′ and 5′-ACTGATAAGCTTTTAGGCCACCTCGGCAAAGAC-3′, cut with *Hin*dIII (Fermentas, St. Leon-Rot, Germany), and ligated with the expression vector pASK-IBA5plus (IBA, Göttingen, Germany) that had been digested with *Ehe*I and *Hin*dIII. As result, PD ω-AT was encoded with an N-terminal *Strep*-tag II[23] under tight transcriptional control of the tetracycline promoter/operator.[24]

Using this expression plasmid, PD ω-AT was produced in *E. coli* BL21[25] in 2 L shake flask cultures with LB medium[26] containing 100 μg/mL ampicillin. Gene expression was induced at OD_{550} = 0.5 with 0.2 μg/mL anhydrotetracycline (aTc; Acros Organics, Geel, Belgium). Three hours after induction the cells were harvested by centrifugation (4200*g*, 20 min, 4°C). After cell disruption in the presence of 25 m*M* Hepes/NaOH, pH 8.3, using a French pressure cell (SLM Aminco, Urbana, IL) PD ω-AT was purified from the soluble extract by affinity chromatography with an engineered streptavidin having reduced biotin affinity immobilized on Activated CH-Sepharose 4B (GE Healthcare, Munich, Germany). After elution with biotin the relevant protein fraction was supplemented with 0.3 m*M* PLP (Roche Diagnostics, Mannheim, Germany) and subjected to size exclusion chromatography (SEC) on a Superdex 200 prep grade HiLoad 16/60 column (GE Healthcare) in the presence of 25 m*M* Hepes/NaOH, pH 8.3. The enzyme eluted from SEC with an apparent molecular size of 86 kDa, indicating formation of a stable homo-dimer. The purified enzyme was analyzed by SDS-PAGE. Protein concentration was determined via UV absorption at 280 nm by means of a calculated extinction coefficient[27] of 66,725 M^{-1} cm^{-1} which included the absorption contribution of PLP (using an extinction coefficient of 1301 M^{-1} cm^{-1} at 280 nm, as measured for the pure compound, and of 3211 M^{-1} cm^{-1} at 390 nm, a wavelength outside the absorption of the protein that allows quantification of the PLP group itself).

Protein crystallization

The purified PD ω-AT was crystallized at 20°C from a 12.5 mg/mL protein solution in 25 m*M* Hepes/NaOH, pH 8.3, in sitting drops using the vapor diffusion technique. Crystals usually appeared within 3 to 5 days after mixing 1 μL protein solution with 1 μL reservoir solution containing 25% (w/v) PEG 3350, 0.2 to 0.4 *M* NaCl, and 0.1 *M* Bis-Tris/HCl, pH 6.5, or 0.1 *M* Tris/HCl, pH 7.0. In particular, needle-shaped crystals of diffraction quality with a smallest dimension of 40 μm were obtained with a reservoir solution containing 25% (w/v) PEG3350, 0.4 *M* NaCl, 10 m*M* urea, and 0.1 *M* Tris/HCl, pH 7.0. These crystals were harvested using Litho-loops (Molecular Dimensions, Newmarket, UK), transferred into reservoir solution supplemented with 30% (v/v) glycerol for cryo-protection, and subsequently flash-frozen in liquid nitrogen.

Table I
X-Ray Crystallographic Statistics

Data collection:	
Space group	$P2_1$
Unit cell parameters	a = 66.79, b = 103.63, c = 145.43 (in Å) and α = 90, β = 98.88, γ = 90 (in °)
Wavelength (Å)	0.9184
Resolution (Å)	20–2.60 (2.70–2.60)[a]
Completeness (%)	99.6 (99.5)
Unique reflections	60,091 (6386)
Multiplicity	3.8 (3.8)
Mean $I/\sigma(I)$	14.3 (2.8)
R_{meas} (%)	11.1 (65.1)
Wilson B-factor (Å^2)	41.0
Refinement:	
Resolution (Å)	19.83–2.60 (2.67–2.60)
Reflections (working)	57,027 (4107)
Reflections (test)	3063 (231)
R_{cryst} (%)	17.8 (25.4)
R_{free} (%)	22.7 (33.0)
No. atoms protein/ligand/ions/waters	13,952/76[b]/4/245
B-values protein/ligand/ions/waters (Å^2)	38.4/46.1/33.1/27.1
Ramachandran plot: favored/outliers (%)[c]	95.1/0.1
Rmsd bonds (Å)/angles (°)	0.008/1.30

[a]Values in parentheses represent the highest resolution shell.
[b]The ligand atoms correspond to the PLP in chains A, B, C, D and 5-aminopentanoate in chains A and C.
[c]The Ramachandran plot was calculated with MolProbity.[35]

X-ray data collection and refinement

Diffraction data was collected at the BESSY Synchrotron (Berlin, Germany) beamline 14.1. The data were indexed, integrated, and scaled in space group $P2_1$ (Table I) with the XDS software package.[29] The unit cell parameters suggested the presence of four polypeptide chains (i.e. a pair of homo-dimers) per asymmetric unit, corresponding to a Matthews coefficient of 2.4 Å^3/Da. In order to solve the structure by molecular replacement, a homology model was built with MODELLER[30] using three X-ray structures of closely homologous ATs (PDB codes: 3GJU, 3I5T, and 3HMU) that were identified using HHpred.[14,15] The PLP cofactor was inserted via superposition with one of the homologous structures (3GJU) using FATCAT.[31] The

resulting model was subjected to refinement with REFMAC5[32] and manually rebuilt in an iterative manner using Coot.[33] At early stages of refinement non-crystallographic symmetry restraints were applied for the mutually equivalent chains A/C and B/D and released later. TLS segments were determined with TLSMD[34] and again refined with REFMAC5. The quality of the resulting protein model was validated with Mol Probity.[35] Molecular graphics were prepared with PyMOL[28] while secondary structure elements were assigned with DSSP.[36] *In silico* screening of the chemical compound library "clean leads" (http://zinc.docking.org/subsets/clean-leads) was performed with DOCK Blaster[37] using default parameters as recommended by the developers (http://blaster.docking.org). The coordinates and structure factors for PD ω-AT have been deposited under accession code 4GRX at the Protein Data Bank at RCSB.

RESULTS AND DISCUSSION

Phylogenetic classification of Class III ATs

Comprehensive bioinformatical analysis of ATs goes back to 1993, when all known AT sequences, that is, 51 sequences of 14 different enzymes from various organisms, were aligned using algorithms for sequence comparison, hydropathy pattern, and secondary structure prediction.[38] These ATs were divided into four subgroups (I–IV) on the basis of their mutual structural relatedness and, therein, the ω-ATs were classified as subgroup II. This heterogeneous classification/denomination still persists in the scientific literature, in parallel to the more recent structure-based classification described further above. In 1996, a first dendrogram was constructed by multiple alignment of amino acid sequences, depicting the evolutionary relationships of 47 proteins belonging to ATs of fold Type I, Class I (cf. Introduction).[39] However, sequences of ω-ATs belonging to the Class III of fold Type I have not been investigated in detail up to now. Consequently, we have carried out a new fundamental analysis of Class III AT sequences, which will be described in the following.

Three hundred thirty nonredundant sequences of Class III ATs, enriched for ω-ATs, were aligned in a structure-guided fashion (see Materials and Methods) using 28 known crystal structures of Class III ATs—sharing up to 70% sequence identity—that were identified with HHpred[14,15] using PD ω-AT as template. Starting from this amino acid sequence alignment, a phylogenetic maximum likelihood tree was calculated to initially assess relevant segregations. Our bioinformatics approach was specifically designed to scrutinize the region of the poorly classified AT members by using the structure-guided mode implemented in T-Coffee.[17] In this way a multiple sequence alignment with the highest possible quality was obtained, considering the generally rather low amino acid sequence identity among the Class III ATs. The tree resulting from this analysis is split into six clades (subtrees) of which the first segregates with a very high bootstrap value of 92% (Fig. 1). Most members of this first clade are functionally well characterized ATs. The remainder of the tree comprises five other clades (2–6), which can be regarded as mutually independent as they are separated by edges with very high bootstrap scores. Notably, in this part of the phylogenetic tree (*S*)-selective ω-ATs with practical utility for the preparation of α-chiral amines are found. However, in contrast to the ATs of the first clade, the natural functions and substrates of most ATs within clades 2–6 have been sparsely characterized.

The members of clade 1 can be divided into groups according to their natural AT substrates, such as putrescine, N-acetylornithine, ornithine, and 4-aminobutyrate. As a member of the putrescine ATs, the enzyme YgjG is capable of transaminating polyamines including putrescine, cadaverine, and spermidine, utilizing α-ketoglutarate, α-ketobutyrate, or pyruvate as amino acceptors.[40] *N*-acetylornithine AT (e.g. sAcOAT from *Salmonella typhimurium*) is one of the key enzymes involved in arginine biosynthesis and catalyzes the reversible conversion of *N*-acetylglutamate γ-semialdehyde to *N*-acetylornithine in the presence of L-glutamate.[41] Ornithine AT (e.g. human OAT), a mitochondrial enzyme, controls the L-ornithine level in tissues by catalyzing the transfer of the δ-amino group of L-ornithine to α-ketoglutarate, yielding L-glutamate γ-semialdehyde.[42] 5-Amino-levulinate, the building block of tetrapyrroles, is synthesized by glutamate-1-semialdehyde aminomutase (GSAM) via the C5 pathway in plants and some bacteria. A distinct feature of the catalytic cycle of GSAM is the isomerization of glutamate-1-semialdehyde to 5-aminolevulinate, which involves an intra-molecular exchange of amino and oxo functions without additional donor/acceptor molecules.[43] The exclusive occurrence of GSAM in the C5 pathway and its absence in mammals make it an interesting target for the selective design of safer herbicides and antimicrobial drugs. The D-phenylglycine AT from *Pseudomonas stutzeri* (D-PhgAT) catalyzes the reversible transamination of D-phenylglycine, an important building block for semi-synthetic penicillins and cephalosporins,[44] or D-4-hydroxyphenylglycine with α-ketoglutarate as amino group acceptor.[45] The diaminobutyrate AT from *Acinetobacter baumannii* (DABA-AT) catalyzes the reaction of L-2,4-diaminobutyrate, which occurs in the peptide antibiotics polymyxin and pseudomyxin as well as in the cell walls of bacteria such as *Corynebacteria* or *Agrococcus jenensis* and in plants, with α-ketoglutarate to L-aspartic β-semialdehyde and L-glutamic acid.[46] Degradation of γ-aminobutyrate (GABA), the major inhibitory neurotransmitter in the mammalian brain, is catalyzed by γ-aminobutyrate AT, which constitutes a pharmaceutical drug target.[47] In *E. coli* GABA is converted into succinic semialdehyde by the enzyme GABA-AT using

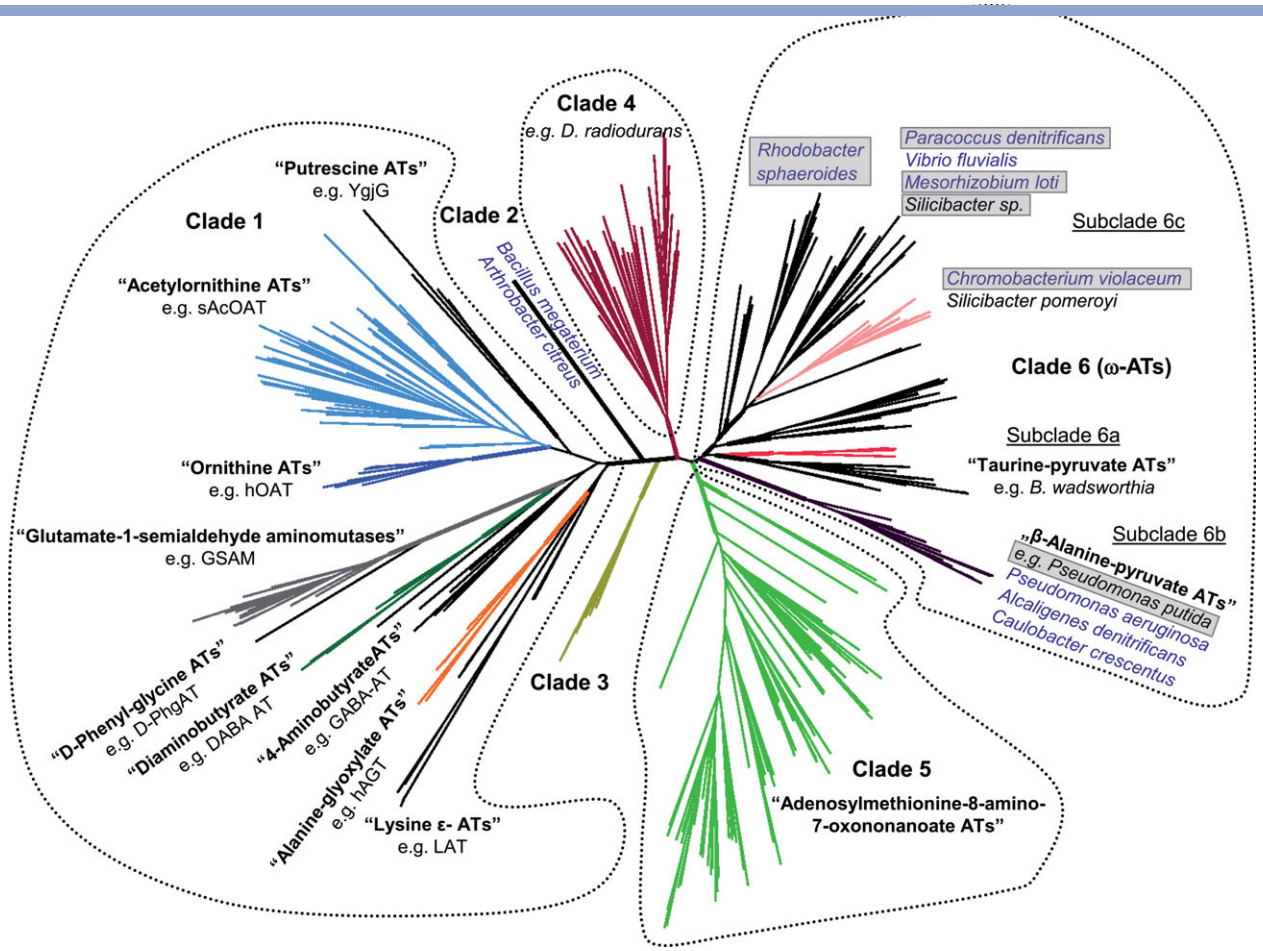

Figure 1

Phylogenetic tree of Class III (ω)-ATs. The members of this family fall into six clades. Generic names of the (*S*)-selective ω-ATs in the right part of the phylogenetic tree, which comprise clades 2–6 and were proven useful for the biotechnological production of chiral amines, are highlighted in blue. Crystal structures in a catalytically active form with the bound PLP cofactor are known for the six framed enzymes (for explanation see text; the full list of ATs is provided in Supporting Information Table SI).

α-ketoglutarate as cosubstrate.[48] The human hepatic peroxisomal alanine-glyoxylate AT (hAGT) is highly specific for converting glyoxylate into glycine with L-alanine as amino group donor, thereby playing a key role in glyoxylate detoxification.[49] Lysine ϵ-AT (LAT), for example, from *Mycobacterium tuberculosis* (PDB code: 2CJG), is involved in lysine metabolism in a wide range of organisms, catalyzing transfer of the ϵ-amino group of lysine to α-ketoglutarate to yield α-aminoadipate δ-semialdehyde and L-glutamate.[50]

Clades 2–6 in the other part(s) of the phylogenetic tree (Fig. 1) predominantly include (*S*)-selective ω-ATs useful for chiral amine production. Within clade 2, which is separated by an edge with 100% bootstrap support, the industrially applied ω-ATs from *Bacillus megaterium* and *Arthrobacter citreus* are found.[51] The (*S*)-specific AT from *Bacillus megaterium* has proven useful for the preparation of (*R*)-1-cyclopropylethylamine and (*R*)-sec-butylamine by kinetic resolution of the racemates.[52] Several thermostable mutants of ω-AT from *Arthrobacter citreus* have been engineered[53,54] and tested in comparison with ω-ATs from *Bacillus megaterium*, *Alcaligenes denitrificans*, *Chromobacterium violaceum*, and *Vibrio fluvialis* for the synthesis of enantiomerically pure amines from the corresponding prochiral aromatic as well as aliphatic ketones (e.g. 4-methoxyphenylacetone and 2-octanone, respectively) by whole-cell catalysis.[55] Clade 3 entirely comprises so far uncharacterized AT enzymes (e.g. UniRef50: C7PTC0, D3T134, A5MZX0,[56] A9WMI0,[57] D0S2L1), separated from the rest of the tree with 96% bootstrap support. An exemplary enzyme for clade 4, which segregates with 100%, is the AT from *Deinococcus radiodurans*.[58] Clade 5, which is separated by 84% bootstrap support, contains adenosylmethionine-8-amino-7-oxononanoate ATs, also known as diaminopelargonic acid synthases (EC 2.6.1.62); examples are the corresponding ATs from *E. coli*, *M. tuberculosis*, and *B. subtilis* (PDB codes: 1QJ3,[59] 3BV0, and 3DU4 as well as

3DOD,[60] respectively). In the pathway of biotin biosynthesis these enzymes catalyze the conversion of 7-keto-8-aminopelargonic acid to 7,8-diaminoperlargonic acid.[59] Finally, clade 6 comprises the most diverse group of ATs in this tree, including important representatives with regard to the biotechnological production of chiral amines, in particular the ω-ATs from *Vibrio fluvialis*,[61] from *Paracoccus denitrificans*,[11,62] and from *Chromobacterium violaceum*.[12]

The subclade 6a, which is separated with a bootstrap value >80%, is represented by the taurine-pyruvate ATs. The corresponding AT from *Bilophila wadsworthia* is able to transaminate taurine, hypotaurine, β-alanine and, with low activity, cysteine as well as 3-aminopropane sulfonate.[63] Apart from pyruvate, 2-ketobutyrate and oxaloacetate are utilized as amino acceptors. The distinct subclade 6b, segregating with 100% bootstrap value, comprises the β-alanine/pyruvate ATs (EC 2.6.1.18). The three-dimensional structure of the corresponding AT from *Pseudomonas putida* has been determined (PDB code: 3A8U).[64] The applicability of the homologous AT from *Pseudomonas aeruginosa* as biocatalyst has been demonstrated by the preparation of a single diastereomer of 2-amino-1,3,4-butanetriol via transamination of L-erythrulose.[65] Another example for this enzyme class is the AT from *Alcaligenes denitrificans* which converts various amino acids and amines into the corresponding keto acids and ketones using pyruvate as amino acceptor.[66] A putative ω-AT gene from *Caulobacter crescentus*, cc3143 (AptA), also grouped into subclade 6b, shows high activity for short-chain β-amino acids.[67] Furthermore, several ω-ATs in subclade 6c, separated by a still significant >67% bootstrap value, appear of practical interest, for example the one from *Vibrio fluvialis*, which catalyzes the synthesis of chiral (*S*)-α-methylbenzylamine (MBA) from acetophenone and L-alanine—upon concomitant removal of pyruvate by lactate dehydrogenase—both in a cell-free extract and by using whole cell biocatalysis.[61] Conversely, the ω-AT from *Chromobacterium violaceum* was shown to convert MBA into acetophenone using pyruvate as cosubstrate.[12] Other examples are the ω-ATs from *Mesorhizobium loti* and *Rhodobacter sphaeroides* that transaminate cyclic ketones.[16] Notably, the ω-AT from *Paracoccus denitrificans* (PD ω-AT) has been applied in a novel biocatalytic production route for the one-pot two-step conversion of L-threonine, involving 2-oxobutyrate as precursor for the transaminase reaction, into L-homoalanine, using benzylamine as cosubstrate.[11] Finally, two members of the subclade 6a, the ω-ATs from *Silicibacter* sp. (PDB code: 3FCR) and *Silicibacter pomeroyi* (PDB code: 3HMU), are so far functionally uncharacterized despite known crystal structures. Notably, there is a huge number of sequences of putative ω-ATs in subclade 6c that are still poorly investigated but, on the basis of our phylogenetic analysis, should have potential for biotechnological processes. Recently, the previously unassigned ω-ATs from *Ochrobactrum anthropi*, *Acinetobacter baumannii*, and *Acetobacter pasteurianus*, all belonging to clade 6 (subclade c, b, and b, respectively), were identified in a BLASTP search using the PD ω-AT as template.[68] These new ω-ATs exhibit similar substrate specificity as PD ω-AT, which led to the hypothesis that the molecular determinants for substrate specificity are generally conserved among ω-ATs. Furthermore, key active site residues were identified by molecular docking simulation using the X-ray structure of the ω-AT from *Pseudomonas putida* (PDB code: 3A8U)[68] which is found in subclade 6b.

Crystal structure of PD ω-AT

PD ω-AT was expressed in *E. coli* and its complex with the covalently bound cofactor PLP was crystallized, followed by X-ray analysis at 2.6 Å resolution (Table I; Fig. 2). The asymmetric unit of the crystal with space group $P2_1$ contained four polypeptide chains that form two canonical AT homo-dimers (A/B and C/D). Interpretable main chain electron density was observed for residues 5 to 453 (last residue) in all four polypeptide chains. The N-terminally appended *Strep*-tag II[23] as well as the four residues following the original start methionine of PD ω-AT were not resolved.

The overall structure of each PD ω-AT subunit exhibits the typical fold Type I.[4] One monomer chain can be subdivided into two distinct domains, a small discontinuous domain comprising residues 1 to 65 together with 344 to 453 and a large domain formed by residues 66 to 343 (Figs. 2 and 3). The N-terminal part of the small domain comprises two α-helices (α1, α2) and three antiparallel β strands (β1–β3) while its C-terminal part contributes a three-stranded antiparallel β-sheet (β11–β13) as well as three α-helices (α12–α14) that lean against it. The large domain consists of a central seven-stranded β-sheet with complex topology (β6-β5-β7-β8-β9-β10-β4), which is mostly parallel, with the exception of strand β10. The β-strands are interconnected by helices α3–α11, which also harbor the cofactor-binding site. Furthermore, each PD ω-AT monomer has a bound sodium ion, which is octahedrally coordinated by the carbonyl oxygens of residues Val101, Glu102, Ser104, and Phe106 as well as up to two water molecules (of which only one is clearly resolved in the electron density). Apparently, the sodium ion stabilizes the loop between helix α4 and strand β4. A similar ion-binding site was reported for the homologous structure of a 7,8-diaminopelargonic acid synthase (27% amino acid sequence identity) from *E. coli* (PDB entry 1QJ3)[59] and for the ω-AT (38% sequence identity) from *Chromobacterium violaceum* (PDB entry 4A6T) mentioned further above.[13]

The electron density for the PLP cofactor is well defined and clearly shows the covalent imino bond with the active site residue Lys285 in the large domain. However, the ideally coplanar conformation of the aldimine

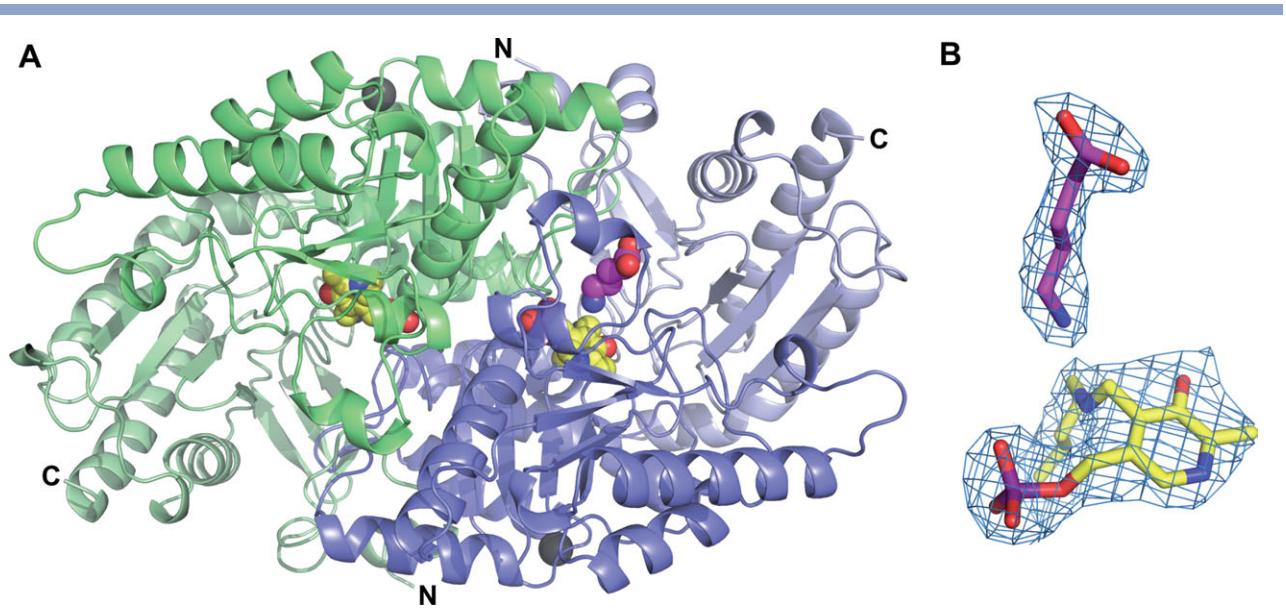

Figure 2

Crystal structure of the PD ω-AT. (**A**) The large domains of the PD ω-AT dimer are colored dark blue (chain A) and dark green (chain B), respectively, while the small domains are colored light blue (chain A) and light green (chain B). PLP (yellow), 5-aminopentanoate in chain A (pink) as well as two sodium ions (grey) are shown in sphere representation. (**B**) 2Fo-Fc electron densities (contoured at 1 σ) are depicted for the ligand 5-aminopentanoate (pink) and the PLP cofactor (yellow) which is bound to the ϵ-nitrogen of Lys285 as a Schiff base.

bond in relation to the pyridine ring is geometrically distorted. Previous publications of the crystal structures of several other PLP-containing enzymes[69–72] have reported this unexpected stereochemistry of the internal aldimine, too, which was interpreted as an X-ray induced deprotonation or reduction of the Lys-PLP Schiff base, thus leading to changes in the molecular geometry.[73,74]

The PLP-binding site of PD ω-AT is located at the interface with the small domain of the same polypeptide chain including contribution by residues from the large domain of the other, opposite subunit [Fig. 2(A)]. Lys285 is located in the loop that connects strands β9 and β10 (Fig. 3). The aromatic ring of PLP is sandwiched between the side chains of Tyr150 and Val258. Its phosphate group is well positioned in the active site through a network of altogether nine hydrogen bonds to four side chains (Ser116, Ser118, Tyr150, and Thr322*; the star denoting the opposite subunit), two backbone amide groups (Gly117, Thr322*), and three water molecules. An almost identical hydrogen bonding network has been described in detail for an ornithine AT (cf. Fig. 1; clade 1) and a 7,8-diaminopelargonic acid synthase (described above; cf. Fig. 1; clade 5) as so-called functional attribute of the phosphate group binding cup of PLP-dependent enzymes.[75] Also, in the aspartate AT family (fold Type I), like in PD ω-AT, the pyridine ring is usually held in place by a hydrogen bond between its nitrogen atom and the side chain carboxylate group of Asp256.[75]

Interestingly, a tubular electron density was observed adjacent to the PLP cofactor within the active sites of chains A and C of PD ω-AT [Fig. 2(B)]. Based on the shape of this density and considering that the ATs from *Vibrio fluvialis* and *Chromobacterium violaceum* possess measurable catalytic activity toward ω-amino-alkanoates as amino donors,[12] the ω-amino (short chain) fatty acid 5-aminopentanoate was modeled into the active site [Figs. 2(B) and 4(A)]. In the resulting complex, 5-aminopentanoate is surrounded by residues Phe19, Tyr150, and Leu417, further to Lys285 with its attached PLP. Considering the close distance of 2.9 Å between the atoms C4' of the coenzyme aldimine and the δ-nitrogen of 5-aminopentanoate, this amino group donor might easily react with PLP in a transamination reaction.

Insights into substrate specificity

On the basis of our high quality crystal structure of the PD ω-AT, we identified by visual inspection altogether 16 essential residues for substrate binding and stereoselectivity [Fig. 4(A)], also encompassing the six residues that were previously identified by molecular docking simulation based on the X-ray structure of the ω-AT from *Pseudomonas putida* (30% sequence identity).[68] Within an 8 Å radius of Lys285 (carrying PLP) the side chains of Asn53, Leu56, Trp57, and Ile259 form the small (S)-pocket, whereas Phe19, Phe85*, Phe86*, Tyr150, Lys163, Tyr165, Ala228, Gly320*, Phe321*, Thr322*, Arg415, and Leu417 shape the large (L)-pocket. L and S designate the two different substrate pockets of a

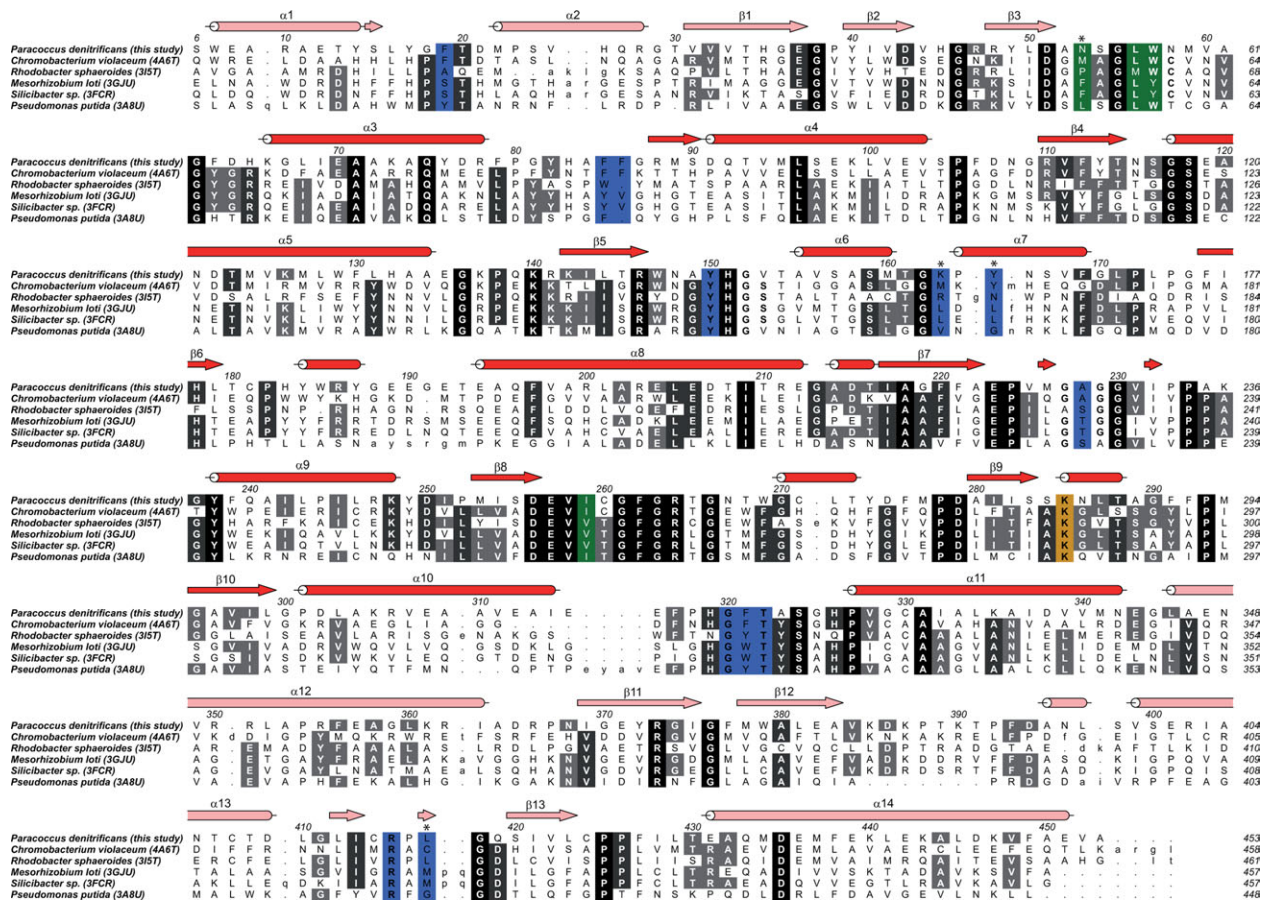

Figure 3

Structure-based sequence alignment between PD ω-AT and five homologous ω-ATs from the subclades 6a and 6c. The PDB codes are given after the name of the source organism. The secondary structures are annotated according to DSSP analysis[36] for PD ω-AT using pink and red colors for the small and large domains, respectively. The catalytically active Lys residue is highlighted in yellow. The identified key active site residues in the large substrate-binding pocket (L) are colored blue, whereas those in the small (S) pocket are colored green, together comprising the "full signature." The specific active-site residues of PD ω-AT, that is Asn53, Lys163, Tyr165, and Leu417 (see text), are labeled with stars. Unaligned residues are printed in lower case.

two-binding site model for VF ω-AT that has been proposed before.[76]

The difference in size of each subpocket and the strong repulsion of the negatively charged carboxylate group in the S pocket have been considered to control substrate specificity and stereoselectivity. The S pocket provides a stringent steric constraint for substrates in most currently available AT enzymes and constitutes a limiting factor for the biocatalytic production of structurally diverse chiral amines.[76] On the other hand, the L pocket shows a dual recognition mode for both hydrophobic groups and polar carboxylate groups, as observed in the side-chain pockets of aspartate AT and aromatic AT.[76] Generally, a dual substrate recognition is essential for the transamination reaction catalyzed by all PLP-dependent ATs and ensures that these enzymes usually can recognize two kinds of substrates that differ in shape and properties within the same active site. ω-ATs, for example, catalyze the reversible transamination reaction in which the α-amino group of an amino acid, for example, the L-alanine cosubstrate, is transferred to PLP to yield PMP and the corresponding α-ketoacid; then, the relevant substrate with an oxo function distal (ω) to the carboxylate group accepts the amino group from PMP to yield the corresponding amine, thus regenerating the coenzyme.

In the following, the 16 essential residues that form the L- and S-substrate pockets of PD ω-AT mentioned above will be termed the "full signature" of ω-ATs. Among those, Tyr150, Thr322*, and Arg415 are highly conserved in the sequences of ω-ATs (Fig. 3). Whilst Tyr150 and Thr322* are identically arranged in space, the orientation of Arg415 differs strongly between chains A(C) and B(D) in the crystal structure. Interestingly, the side chain conformation of Arg415, which is located in the small domain of PD ω-AT, depends on the presence of the 5-aminopentanoate ligand/substrate in the active

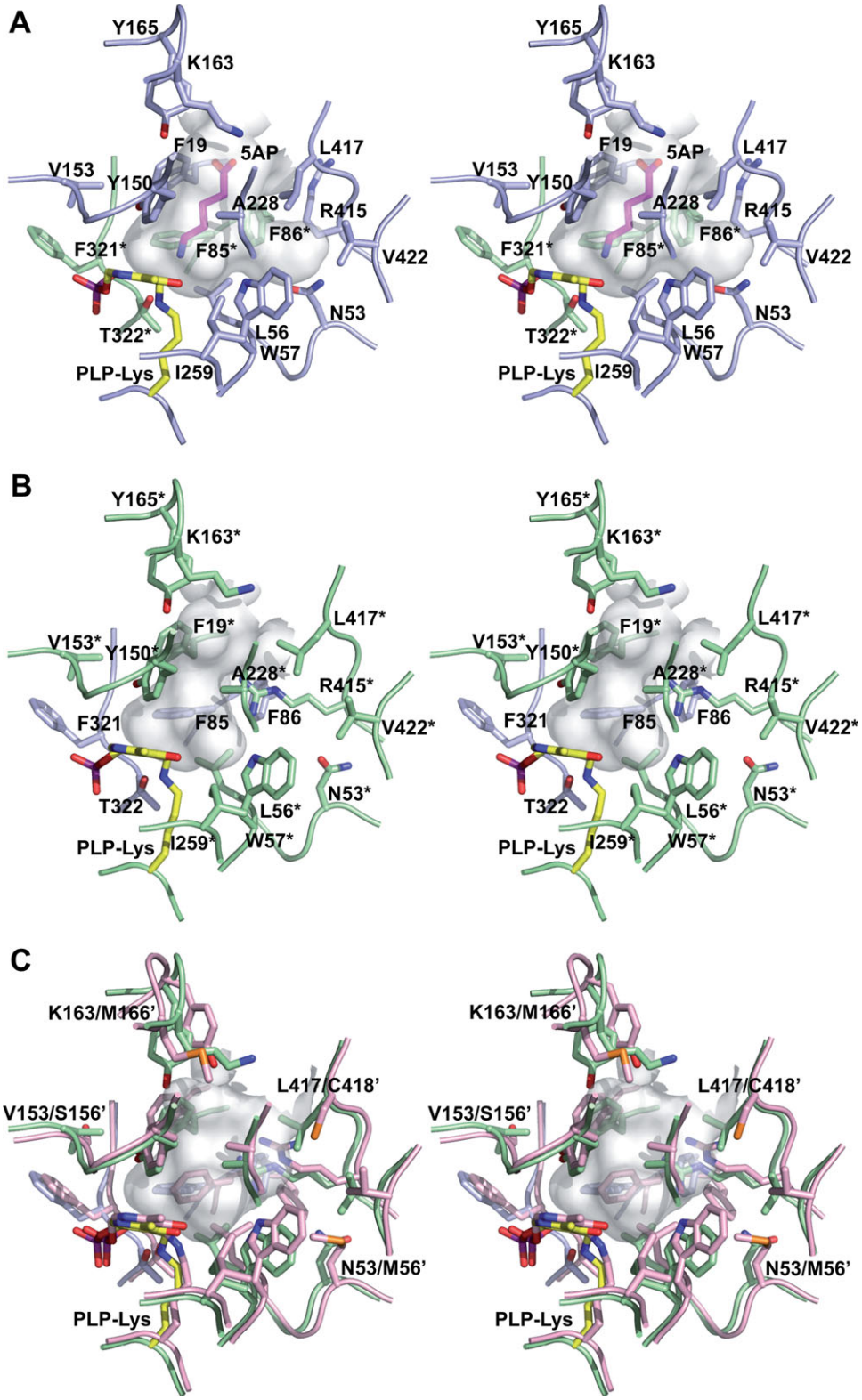

Figure 4

The active site of PD ω-AT and its comparison with CV ω-AT. (**A**) Illustration of the PD ω-AT active site in stereo view. Residues of chain A are highlighted in blue and residues of chain B are highlighted in green (labeled with *). PLP (yellow) and 5-aminopentanoate (5AP) in chain A (pink) are shown as sticks. (**B**) Illustration of the second PD ω-AT active site pocket (chain pair B/A). (**C**) Comparison with the active site of CV ω-AT (labeled with '). Residues of chains A and B of the CV ω-AT are both highlighted in pink. Hetero-atom coloring is shown for nitrogen (blue), oxygen phosphor (purple) and sulfur (orange).

site [Fig. 4(A)]. In subunit A, where the ligand is bound, Arg415 points away from its carboxylate group—resulting in a distance of more than 8 Å—and the active site pocket appears expanded [Fig. 4(A)]. Conversely, in subunit B, which does not show corresponding ligand density, the side chain of Arg415 adopts a conformation that would allow interaction with a bound (small) substrate and the active site pocket appears closed, resembling that of the CV ω-AT, for example [Fig. 4(B,C)].

This observed conformational change in subunit A of PD ω-AT is caused by a movement of the small domain in relation to the large domain and leads to a significantly altered tilt angle of 2° between both domains of subunit A compared with those of subunit B. Contrasting, the tilt angle is almost unaltered in the CV ω-AT, with 0.6° change between the corresponding domains of chains A and B. It is known that fold Type I ATs show various degrees of overall change in conformation depending upon substrate binding, which is most likely due to divergent evolution of the ancestor protein of fold Type I enzymes.[77] The aromatic amino acid AT (AroAT) from *Paracoccus denitrificans*, for example, changes its conformation from an open to a closed form upon substrate binding.[78] In contrast, the acetylornithine AT from *Thermus thermophilus*, clearly related in sequence to PD ω-AT (26% amino acid identity; cf. Fig. 1), exhibits no significant change in overall conformation and active-site structure in the substrate-free form versus its complexes with acetylornithine or glutamate.[77] The common feature of fold Type I ATs is that all enzyme-substrate complexes show a similar overall structure and active-site main chain conformation, regardless of the kind of bound substrate. Thus, it appears that the obviously larger active site pocket of PD ω-AT in the presence of the putative ligand 5-aminopentanoate actually resembles the open form that is generally adopted upon substrate binding [Fig. 4(A)].

Five aromatic side chains within the active site of PD ω-AT, Phe19, Phe85*, Phe86*, Tyr150, and Tyr165, provide a hydrophobic environment to accommodate an aromatic substrate in the L-pocket, probably also contributing π-stacking interactions. In comparison with other ω-ATs, the most variable sequence position in relation to PD ω-AT is Tyr165, followed by Phe19 [Fig. 4(A)]. Notably, with the exception of Tyr150, all aromatic side chains are adjacent to glycine or proline residues (Gly18/Phe19; Phe85*/86*/Gly87*; Pro164/Tyr165), which have a strong—in fact, mutually opposing—influence on the polypeptide backbone flexibility. This observation indicates a special role of these residues for substrate binding and explains the well documented preference of PD ω-AT for aromatic substrates, such as (*S*)-1-aminoindane, (*S*)-α-methylbenzylamine, and benzylamine.[68] Apart from this experimentally proven specificity, a bioinformatics analysis of the potential substrate range of PD ω-AT using DOCK Blaster with a dataset of 737,685 compounds (see Material and Methods) resulted in 100 top scoring compounds that almost all carried an aromatic ring structure.

In a parallel bioinformatics analysis, amino acid determinants for the substrate specificity of ω-ATs were identified using SDPpred[79] and Comulator[80] on the basis of the multiple sequence alignment generated in context of our phylogenetic analysis (Fig. 1). SDPpred searches for positions that are well conserved within groups of sequences with the same specificity (here within each of the six clades) but differ between them, so-called specificity-determining positions (SDPs). Comulator, on the other hand, indicates correlated mutations, that is pairs of residues (columns) in a multiple alignment that are mutually dependent with regard to the acquisition of mutations, without requiring previous manual grouping of sequences. As result, five of the seven top scoring residues from the Comulator analysis coincided with five of the seven top scoring subtyping residues from SDPpred: Leu56, Ile259, and Ala228 located close to the active site and, furthermore, Val153 and Phe321*. Val153 is situated adjacent to the phosphate group of PLP at the interface of the two enzyme subunits and at a distance of 3.5 Å from Phe321*. Apart from that, SDPpred detected Trp57 and Gly55 neighboring Leu56 [cf. Fig. 4(A)]. Notably, with the exception of Val153 and Gly55, the predicted amino acid residues are part of the "full signature" of ω-ATs that was elucidated during our structural analysis explained above. However, considering the crystal structure of PD ω-AT, a contribution of these latter two residues to the specificity of the active site pocket is unlikely [cf. Fig. 4(A)].

Comparison of PD ω-AT with closely related Class III ATs

In a search with DALI[81] the following nine close structural homologs of PD ω-AT were identified: ω-AT from *Vibrio fluvialis* (3NUI; *Z*-score 59.5%; 92% amino acid sequence identity), ω-AT from *Mesorhizobium loti* (3GJU; *Z*-score 53.7; 31% identity), ω-AT from *Silicibacter* sp. (3FCR; *Z*-score 53.3; 32% identity), ω-AT from *Chromobacterium violaceum* (4A6T; *Z*-score 51.5; 37% identity), ω-AT from *Silicibacter pomeroyi* (3HMU; *Z*-score 51.3; 34% identity), adenosylmethionine-8-amino-7-oxononanoate AT from *Bacillus subtilis* (3DU4; *Z*-score 50.4; 28% identity), ω-AT from *Rhodobacter sphaeroides* (3I5T; *Z*-score 50.6; 32% identity), adenosylmethionine-8-amino-7-oxononanoate AT from *Bacillus anthracis* (3N5M; *Z*-score 49.3; 31% identity), and ω-AT from *Pseudomonas putida* (3A8U; *Z*-score 48.9; 30% identity). Seven of these enzymes belong to the group of ω-ATs. Among those the crystal structures of the ω-ATs from *C. violaceum* (4A6T), *R. sphaeroides* (3I5T), *M. loti* (3GJU), *Silicibacter* sp. (3FCR), and *P. putida* (3A8U) were solved in a catalytically active form with the covalently

bound PLP coenzyme. Notably, with exception of the latter two enzymes these ATs are biotechnologically relevant for the production of chiral amines.[12,16]

The PD ω-AT was compared in a structure-based sequence alignment with these five enzymes (Fig. 3). In addition, PD ω-AT was superimposed with the CV ω-AT, which provides the most closely related crystal structure (despite just 38% sequence identity) containing the PLP cofactor [Fig. 4(C)]. Of the 16 residues identified for PD ω-AT above ("full signature" of ω-ATs) the following three differ from CV ω-AT: Asn53 (Met56 in CV ω-AT), Lys163 (Met166), and Leu417 (Cys418). These structural changes lead to clearly modified properties of the active site with regard to hydrophobicity and charge, thus increasing the nonpolar character of the active site in CV ω-AT. Furthermore, significant differences in side chain conformation were found for the mutually conserved residues Arg415(416), Phe85*(88*), and Phe86*(89*). The modified orientations of the aromatic side chains of Phe85* and Phe86* in PD ω-AT appear to be a consequence of a peptide flip between both residues, which is caused by the differing neighboring residues His83 (Asn86) and Arg88 (Thr91). The relevance of residue Arg415 in PD ω-AT for the recognition of the substrate carboxylate group was already discussed above.

In conclusion of the structural comparison between PD ω-AT and CV ω-AT, it seems that (i) the available space in the active site is larger for the CV ω-AT, (ii) the hydrophobicity is higher for CV ω-AT, whereas (iii) PD ω-AT provides more possibilities for polar interactions. These observations are consistent with the differences in amino donor and acceptor specificities of both enzymes.[11,12] Generally, CV ω-AT has higher activity for benzyl/phenyl compounds (such as 1-methyl-3-phenylpropylamine as donor or phenyl acetaldehyde as acceptor) as well as aliphatic substrates (such as 6-aminohexanoic acid as donor or nonanal as acceptor) with longer chain length.

Potential of ω-ATs for industrial biotechnology

As a result of our comprehensive phylogenetic analysis (Fig. 1) it becomes evident that the most important representatives of ω-ATs with potential for the biotechnological production of chiral amines are clustered in clade 6 of the Class III ATs, thus including the PD ω-AT and the CV ω-AT. Within this clade a huge number of sequences of putative ω-ATs are still uncharacterized but show promise for industrial application. Recently, for example, ω-ATs from *Ochrobactrum anthropi*, *Acinetobacter baumannii*, and *Acetobacter pasteurianus* were identified by a BLASTP search using the PD ω-AT (see above).[68] Their subsequent functional characterization revealed[68] that all three enzymes exhibit a similar substrate specificity as the PD ω-AT, therefore in principle suggesting suitability for the production of amines in industrial processes.

The set of 16 essential residues for substrate specificity, the "full signature" of ω-ATs that has been identified on the basis of the new crystal structure of PD ω-AT as well as use of SDPpred and Comulator together with our phylogenetic analysis, should aid in spotting further candidates for biotechnologically applicable ATs. Among the "full signature" especially residues Asn53, Lys163, Tyr165, and Leu417 are important for substrate and stereo-specificity of PD ω-AT. On the other hand, the amino acid positions Phe19, Leu56, Trp57, Phe85*, Phe86*, Ile259, Tyr150, Ala228, Gly320*, Phe321*, Thr322*, and Arg415 seem to be relevant for substrate recognition within the entire family of ω-ATs and therefore appear important for their classification. This reduced set of 12 active site residues will be referred to as the "partial signature" of ω-ATs.

Four positions in this "partial signature"—Trp57, Phe85*, Tyr150, and Ala228 were previously studied by site-directed mutagenesis of VF ω-AT[82] and CV ω-AT[83] in attempts to redesign the substrate specificity and to understand the enantioselectivity preference of ω-ATs. The mutation Trp57Gly in VF ω-AT resulted in improved catalytic activities for aromatic and aliphatic amines without compromising enantioselectivity. The mutation Trp60Ala in CV ω-AT (equivalent to Trp57 in PD ω-AT) slightly improved the enantiospecificity for the conversion of 2-aminotetralin, whereas corresponding values for 1-phenylethylamine and 1-aminotetralin were drastically reduced. In contrast, the mutation Trp60Cys gave rise to improved enantiospecificities for all three substrates. The double mutation Phe88Ala/Ala231Phe (positions Phe85* and Ala228 in PD ω-AT) led to a substrate-dependent shift in enantiopreference. Furthermore, the site of PLP attachment was shifted in the CV ω-AT variant Tyr153Lys/Lys288Tyr. Hence, the four active site residues mentioned above were experimentally demonstrated to possess significant influence on catalytic activity, substrate specificity, and enantiomeric preference of ω-ATs.

From the multiple alignment of overall 330 Class III AT sequences, constituting the basis of our phylogenetic tree, eight known ω-ATs and two previously unassigned ω-ATs that exhibit the "partial signature" (Supporting Information Fig. S1) were identified. Except for a γ-aminobutyrate AT from *Arabidopsis thaliana* (UniProt ID Q94FS9),[84] all these ω-ATs are of bacterial origin. The two previously unassigned ω-ATs originate from *Pseudomonas stutzeri* (F8H3E0) and from *Pseudomonas putida* (F8FY58).[85] The specific residues Asn53, Lys163, Tyr165, and Leu417 of PD ω-AT, which complement the set of amino acids for the "full signature," were only found in the ω-ATs from *Vibrio fluvialis*, from *Rhodobacter sphaeroides* and from *Mesorhizobium* sp.[16,61] Notably, the potential of these three ATs for the production of chiral amines has already been demonstrated (see further above). Accordingly, the 12 key residues of the "partial signature" should be helpful to quickly identify further

ω-AT candidates for industrial application when searching new sequences. The probability that these ω-ATs catalyze the formation of chiral amines should be high.

Taken together, the ω-ATs from *Chromobacterium violaceum*, from *Vibrio fluvialis*, and from *Paracoccus denitrificans*, which already have been applied for the biocatalytic preparation of amines, all exhibit the 12 identified active site residues from the "partial signature."[11,12,51,68] These ω-ATs show high activity towards the amino acceptors pyruvate, hydroxypyruvate, glyoxylate, butanal, hexanal, and benzaldehyde and toward the amino donors benzylamine, (*S*)-α-methylbenzylamine, and (*S*)-1-aminoindane. Moreover, these ω-ATs are characterized by a distinct set of five to six aromatic amino acids in their active sites. Consequently, we assume that the two ω-ATs from *Pseudomonas stutzeri* and *Pseudomonas putida* proposed on the basis of our analysis should show a similar preference for aromatic substrates and constitute new promising candidates for the industrial production of corresponding chiral amines.

ACKNOWLEDGMENTS

The authors thank Evonik, in particular Kai Doderer, for providing the PD ω-AT gene. The authors also thank Uwe Müller and Manfred Weiss for technical support at MX beamline 14.1 of the Helmholtz-Zentrum Berlin—Electron Storage Ring BESSY II (Berliner Elektronenspeicherring-Gesellschaft für Synchrotronstrahlung, Berlin, Germany, and Free University Berlin at BESSY).

REFERENCES

1. Alexander FW, Sandmeier E, Mehta PK, Christen P. Evolutionary relationships among pyridoxal-5'-phosphate-dependent enzymes. Regio-specific α, β and γ families. Eur J Biochem 1994;219:953–960.
2. Eliot AC, Kirsch JF. Pyridoxal phosphate enzymes: mechanistic, structural, and evolutionary considerations. Annu Rev Biochem 2004;73:383–415.
3. Jansonius JN. Structure, evolution and action of vitamin B6-dependent enzymes. Curr Opin Struct Biol 1998;8:759–769.
4. Grishin NV, Phillips MA, Goldsmith EJ. Modeling of the spatial structure of eukaryotic ornithine decarboxylases. Protein Sci 1995;4:1291–1304.
5. Percudani R, Peracchi A. The B6 database: a tool for the description and classification of vitamin B6-dependent enzymatic activities and of the corresponding protein families. BMC Bioinformatics 2009;10:273.
6. Punta M, Coggill PC, Eberhardt RY, Mistry J, Tate J, Boursnell C, Pang N, Forslund K, Ceric G, Clements J, Heger A, Holm L, Sonnhammer EL, Eddy SR, Bateman A, Finn RD. The Pfam protein families database. Nucleic Acids Res 2012;40:D290–D301.
7. Rudat J, Brucher BR, Syldatk C. Transaminases for the synthesis of enantiopure β-amino acids. AMB Express 2012;2:11.
8. Malik MS, Park ES, Shin JS. Features and technical applications of ω-transaminases. Appl Microbiol Biotechnol 2012;94:1163–1171.
9. Tufvesson P, Lima-Ramos J, Jensen JS, Al-Haque N, Neto W, Woodley JM. Process considerations for the asymmetric synthesis of chiral amines using transaminases. Biotechnol Bioeng 2011;108:1479–1493.
10. Yun H, Cho BK, Kim BG. Kinetic resolution of (R,S)-sec-butylamine using ω-transaminase from *Vibrio fluvialis* JS17 under reduced pressure. Biotechnol Bioeng 2004;87:772–778.
11. Park E, Kim M, Shin J-S. One-pot conversion of L-threonine into L-homoalanine: biocatalytic production of an unnatural amino acid from a natural one. Adv Synth Catal 2010;352:3391–3398.
12. Kaulmann U, Smithies K, Smith MEB, Hailes HC, Ward JM. Substrate spectrum of ω-transaminase from *Chromobacterium violaceum* DSM30191 and its potential for biocatalysis. Enzyme Microbial Technol 2007;41:628–637.
13. Humble MS, Cassimjee KE, Hakansson M, Kimbung YR, Walse B, Abedi V, Federsel HJ, Berglund P, Logan DT. Crystal structures of the *Chromobacterium violaceum* ω-transaminase reveal major structural rearrangements upon binding of coenzyme PLP. FEBS J 2012;279:779–792.
14. Söding J, Biegert A, Lupas AN. The HHpred interactive server for protein homology detection and structure prediction. Nucleic Acids Res 2005;33:W244–W248.
15. Biegert A, Mayer C, Remmert M, Söding J, Lupas AN. The MPI Bioinformatics Toolkit for protein sequence analysis. Nucleic Acids Res 2006;34:W335–W339.
16. Sieber V, Grammann K, Rühmann B, Haas T, Pfeffer JC, Doderer K, Rollmann C, Skerra A, Rausch C, Lerchner A. Method for the amination of polycyclic compounds using transaminases. WO2010/089171.
17. Notredame C, Higgins DG, Heringa J. T-Coffee: a novel method for fast and accurate multiple sequence alignment. J Mol Biol 2000;302:205–217.
18. Stamatakis A. RAxML-VI-HPC: maximum likelihood-based phylogenetic analyses with thousands of taxa and mixed models. Bioinformatics 2006;22:2688–2690.
19. Eddy SR. Accelerated profile HMM searches. PLoS Comput Biol 2011;7:e1002195.
20. Uniprot-Consortium. The universal protein resource (UniProt). Nucleic Acids Res 2007;35:D193–D197.
21. Boeckmann B, Bairoch A, Apweiler R, Blatter MC, Estreicher A, Gasteiger E, Martin MJ, Michoud K, O'Donovan C, Phan I, Pilbout S, Schneider M. The SWISS-PROT protein knowledgebase and its supplement TrEMBL in 2003. Nucleic Acids Res 2003;31:365–370.
22. Bond CS, Schüttelkopf AW. ALINE: a WYSIWYG protein-sequence alignment editor for publication-quality alignments. Acta Crystallogr D Biol Crystallogr 2009;65:510–512.
23. Schmidt TG, Skerra A. The *Strep*-tag system for one-step purification and high-affinity detection or capturing of proteins. Nat Protoc 2007;2:1528–1535.
24. Skerra A. Use of the tetracycline promoter for the tightly regulated production of a murine antibody fragment in *Escherichia coli*. Gene 1994;151:131–135.
25. Studier FW, Moffatt BA. Use of bacteriophage T7 RNA polymerase to direct selective high-level expression of cloned genes. J Mol Biol 1986;189:113–130.
26. Sambrook J, Russell DW. Molecular cloning: a laboratory manual. Cold Spring Harbor, NY: Cold Spring Harbor Laboratory Press; 2001.
27. Gasteiger E, Hoogland C, Gattiker A, Duvaud S, Wilkins MR, Appel RD, Bairoch A. Protein identification and analysis tools on the ExPASy server. In: Walker JM, editor. The Proteomics Protocols Handbook. NY: Humana Press; 2005, pp 571–607.
28. DeLano WL. The PyMOL molecular graphics system. San Carlos, CA: DeLano Scientific; 2002.
29. Kabsch W. XDS. Acta Crystallogr D Biol Crystallogr 2010;66:125–132.
30. Eswar N, Webb B, Marti-Renom MA, Madhusudhan MS, Eramian D, Shen MY, Pieper U, Sali A. Comparative protein structure modeling using MODELLER. Curr Protoc Protein Sci 2007;50:2.9.1–2.9.31.
31. Ye Y, Godzik A. Flexible structure alignment by chaining aligned fragment pairs allowing twists. Bioinformatics 2003;19 (Suppl 2):ii246–ii255.
32. Murshudov GN, Skubak P, Lebedev AA, Pannu NS, Steiner RA, Nicholls RA, Winn MD, Long F, Vagin AA. REFMAC5 for the

refinement of macromolecular crystal structures. Acta Crystallogr D Biol Crystallogr 2011;67:355–367.
33. Emsley P, Lohkamp B, Scott WG, Cowtan K. Features and development of Coot. Acta Crystallogr D Biol Crystallogr 2010;66:486–501.
34. Painter J, Merritt EA. TLSMD web server for the generation of multi-group TLS models. J Appl Cryst 2006;39:109–111.
35. Davis IW, Leaver-Fay A, Chen VB, Block JN, Kapral GJ, Wang X, Murray LW, Arendall WB, III, Snoeyink J, Richardson JS, Richardson DC. MolProbity: all-atom contacts and structure validation for proteins and nucleic acids. Nucleic Acids Res 2007;35:W375–W383.
36. Kabsch W, Sander C. Dictionary of protein secondary structure: pattern recognition of hydrogen-bonded and geometrical features. Biopolymers 1983;22:2577–2637.
37. Irwin JJ, Shoichet BK, Mysinger MM, Huang N, Colizzi F, Wassam P, Cao Y. Automated docking screens: a feasibility study. J Med Chem 2009;52:5712–5720.
38. Mehta PK, Hale TI, Christen P. Aminotransferases: demonstration of homology and division into evolutionary subgroups. Eur J Biochem 1993;214:549–561.
39. Jensen RA, Gu W. Evolutionary recruitment of biochemically specialized subdivisions of Family I within the protein superfamily of aminotransferases. J Bacteriol 1996;178:2161–2171.
40. Samsonova NN, Smirnov SV, Altman IB, Ptitsyn LR. Molecular cloning and characterization of *Escherichia coli* K12 *ygjG* gene. BMC Microbiol 2003;3:2.
41. Rajaram V, Ratna Prasuna P, Savithri HS, Murthy MR. Structure of biosynthetic *N*-acetylornithine aminotransferase from *Salmonella typhimurium*: studies on substrate specificity and inhibitor binding. Proteins 2008;70:429–441.
42. Storici P, Capitani G, Müller R, Schirmer T, Jansonius JN. Crystal structure of human ornithine aminotransferase complexed with the highly specific and potent inhibitor 5-fluoromethylornithine. J Mol Biol 1999;285:297–309.
43. Orriss GL, Patel TR, Sorensen J, Stetefeld J. Absence of a catalytic water confers resistance to the neurotoxin gabaculine. FASEB J 2010;24:404–414.
44. Müller U, van Assema F, Gunsior M, Orf S, Kremer S, Schipper D, Wagemans A, Townsend CA, Sonke T, Bovenberg R, Wubbolts M. Metabolic engineering of the *E. coli* L-phenylalanine pathway for the production of D-phenylglycine (D-Phg). Metab Eng 2006; 8:196–208.
45. Wiyakrutta S, Meevootisom V. A stereo-inverting D-phenylglycine aminotransferase from *Pseudomonas stutzeri* ST-201: purification, characterization and application for D-phenylglycine synthesis. J Biotechnol 1997;55:193–203.
46. Ikai H, Yamamoto S. Identification and analysis of a gene encoding L-2,4-diaminobutyrate:2-ketoglutarate 4-aminotransferase involved in the 1,3-diaminopropane production pathway in *Acinetobacter baumannii*. J Bacteriol 1997;179:5118–5125.
47. Sarup A, Larsson OM, Schousboe A. GABA transporters and GABA-transaminase as drug targets. Curr Drug Targets CNS Neurol Disord 2003;2:269–277.
48. Liu W, Peterson PE, Carter RJ, Zhou X, Langston JA, Fisher AJ, Toney MD. Crystal structures of unbound and aminooxyacetate-bound *Escherichia coli* γ-aminobutyrate aminotransferase. Biochemistry 2004;43:10896–10905.
49. Cellini B, Bertoldi M, Montioli R, Paiardini A, Borri Voltattorni C. Human wild-type alanine:glyoxylate aminotransferase and its naturally occurring G82E variant: functional properties and physiological implications. Biochem J 2007;408:39–50.
50. Mani Tripathi S, Ramachandran R. Direct evidence for a glutamate switch necessary for substrate recognition: crystal structures of lysine ϵ-aminotransferase (Rv3290c) from *Mycobacterium tuberculosis* H37Rv. J Mol Biol 2006;362:877–886.
51. Koszelewski D, Tauber K, Faber K, Kroutil W. ω-transaminases for the synthesis of non-racemic α-chiral primary amines. Trends Biotechnol 2010;28:324–332.
52. Hanson RL, Davis BL, Chen Y, Goldberg SL, Parker WL, Tully TP, Montana MA, Patel RN. Preparation of (*R*)-amines from racemic amines with an (*S*)-amine transaminase from *Bacillus megaterium*. Adv Synth Catal 2008;350:1367–1375.
53. Martin AR, DiSanto R, Plotnikov I, Kamat S, Shonnard D, Pannuri S. Improved activity and thermostability of (*S*)-aminotransferase by error-prone polymerase chain reaction for the production of a chiral amine. Biochem Eng J 2007;37:246–255.
54. Pannuri S, Kamat SV, Garcia ARM. Thermostable ω-transaminases. WO2006/063336.
55. Koszelewski D, Göritzer M, Clay D, Seisser B, Kroutil W. Synthesis of optically active amines employing recombinant ω-transaminases in *E. coli* cells. ChemCatChem 2010;2:73–77.
56. Seedorf H, Fricke WF, Veith B, Brüggemann H, Liesegang H, Strittmatter A, Miethke M, Buckel W, Hinderberger J, Li F, Hagemeier C, Thauer RK, Gottschalk G. The genome of *Clostridium kluyveri*, a strict anaerobe with unique metabolic features. Proc Natl Acad Sci USA 2008;105:2128–2133.
57. Wiens GD, Rockey DD, Wu Z, Chang J, Levy R, Crane S, Chen DS, Capri GR, Burnett JR, Sudheesh PS, Schipma MJ, Burd H, Bhattacharyya A, Rhodes LD, Kaul R, Strom MS. Genome sequence of the fish pathogen *Renibacterium salmoninarum* suggests reductive evolution away from an environmental *Arthrobacter* ancestor. J Bacteriol 2008;190:6970–6982.
58. Chen CD, Huang TF, Lin CH, Guan HH, Hsieh YC, Lin YH, Huang YC, Liu MY, Chang WC, Chen CJ. Purification, crystallization and preliminary X-ray crystallographic analysis of branched-chain aminotransferase from *Deinococcus radiodurans*. Acta Crystallogr Sect F Struct Biol Cryst Commun 2007;63:492–494.
59. Käck H, Sandmark J, Gibson K, Schneider G, Lindqvist Y. Crystal structure of diaminopelargonic acid synthase: evolutionary relationships between pyridoxal-5'-phosphate-dependent enzymes. J Mol Biol 1999;291:857–876.
60. Dey S, Lane JM, Lee RE, Rubin EJ, Sacchettini JC. Structural characterization of the *Mycobacterium tuberculosis* biotin biosynthesis enzymes 7,8-diaminopelargonic acid synthase and dethiobiotin synthetase. Biochemistry 2010;49:6746–6760.
61. Shin JS, Kim BG. Asymmetric synthesis of chiral amines with ω-transaminase. Biotechnol Bioeng 1999;65:206–211.
62. Mutti FG, Fuchs CS, Pressnitz D, Turrini NG, Sattler JH, Lerchner A, Skerra A, Kroutil W. Amination of ketones by employing two new (S)-selective ω-transaminases and the His-tagged ω-TA from *Vibrio fluvialis*. Eur J Org Chem 2012;2012:1003–1007.
63. Laue H, Cook AM. Biochemical and molecular characterization of taurine:pyruvate aminotransferase from the anaerobe *Bilophila wadsworthia*. Eur J Biochem 2000;267:6841–6848.
64. Watanabe N, Sakabe K, Sakabe N, Higashi T, Sasaki K, Aibara S, Morita Y, Yonaha K, Toyama S, Fukutani H. Crystal structure analysis of ω-amino acid:pyruvate aminotransferase with a newly developed Weissenberg camera and an imaging plate using synchrotron radiation. J Biochem 1989;105:1–3.
65. Ingram CU, Bommer M, Smith ME, Dalby PA, Ward JM, Hailes HC, Lye GJ. One-pot synthesis of amino-alcohols using a de-novo transketolase and β-alanine:pyruvate transaminase pathway in *Escherichia coli*. Biotechnol Bioeng 2007;96:559–569.
66. Yun H, Lim S, Cho BK, Kim BG. ω-amino acid:pyruvate transaminase from *Alcaligenes denitrificans* Y2k-2: a new catalyst for kinetic resolution of β-amino acids and amines. Appl Environ Microbiol 2004;70:2529–2534.
67. Hwang BY, Ko SH, Park HY, Seo JH, Lee BS, Kim BG. Identification of ω-aminotransferase from *Caulobacter crescentus* and site-directed mutagenesis to broaden substrate specificity. J Microbiol Biotechnol 2008;18:48–54.
68. Park ES, Kim M, Shin JS. Molecular determinants for substrate selectivity of ω-transaminases. Appl Microbiol Biotechnol 2012;93:2425–2435.
69. Krupka HI, Huber R, Holt SC, Clausen T. Crystal structure of cystalysin from *Treponema denticola*: a pyridoxal 5'-phosphate-dependent protein acting as a haemolytic enzyme. EMBO J 2000;19:3168–3178.

70. Ura H, Nakai T, Kawaguchi SI, Miyahara I, Hirotsu K, Kuramitsu S. Substrate recognition mechanism of thermophilic dual-substrate enzyme. J Biochem 2001;130:89–98.
71. Noland BW, Newman JM, Hendle J, Badger J, Christopher JA, Tresser J, Buchanan MD, Wright TA, Rutter ME, Sanderson WE, Müller-Dieckmann HJ, Gajiwala KS, Buchanan SG. Structural studies of *Salmonella typhimurium* ArnB (PmrH) aminotransferase: a 4-amino-4-deoxy-L-arabinose lipopolysaccharide-modifying enzyme. Structure 2002;10:1569–1580.
72. Weyand M, Schlichting I, Herde P, Marabotti A, Mozzarelli A. Crystal structure of the $\beta Ser^{178} \rightarrow Pro$ mutant of tryptophan synthase. A "knock-out" allosteric enzyme. J Biol Chem 2002;277:10653–10660.
73. Hayashi H, Mizuguchi H, Kagamiyama H. The imine-pyridine torsion of the pyridoxal 5'-phosphate Schiff base of aspartate aminotransferase lowers its pK_a in the unliganded enzyme and is crucial for the successive increase in the pK_a during catalysis. Biochemistry 1998;37:15076–15085.
74. Dubnovitsky AP, Ravelli RB, Popov AN, Papageorgiou AC. Strain relief at the active site of phosphoserine aminotransferase induced by radiation damage. Protein Sci 2005;14:1498–1507.
75. Denesyuk AI, Denessiouk KA, Korpela T, Johnson MS. Functional attributes of the phosphate group binding cup of pyridoxal phosphate-dependent enzymes. J Mol Biol 2002;316:155–172.
76. Shin JS, Kim BG. Exploring the active site of amine:pyruvate aminotransferase on the basis of the substrate structure-reactivity relationship: how the enzyme controls substrate specificity and stereoselectivity. J Org Chem 2002;67:2848–2853.
77. Hirotsu K, Goto M, Okamoto A, Miyahara I. Dual substrate recognition of aminotransferases. Chem Rec 2005;5:160–172.
78. Okamoto A, Ishii S, Hirotsu K, Kagamiyama H. The active site of *Paracoccus denitrificans* aromatic amino acid aminotransferase has contrary properties: flexibility and rigidity. Biochemistry 1999;38:1176–1184.
79. Kalinina OV, Mironov AA, Gelfand MS, Rakhmaninova AB. Automated selection of positions determining functional specificity of proteins by comparative analysis of orthologous groups in protein families. Protein Sci 2004;13:443–456.
80. Kuipers RK, Joosten HJ, Verwiel E, Paans S, Akerboom J, van der Oost J, Leferink NG, van Berkel WJ, Vriend G, Schaap PJ. Correlated mutation analyses on super-family alignments reveal functionally important residues. Proteins 2009;76:608–616.
81. Holm L, Rosenstrom P. Dali server: conservation mapping in 3D. Nucleic Acids Res 2010;38:W545–W549.
82. Cho B-K, Park H-Y, Seo J-H, Kim J, Kang T-J, Lee B-S, Kim B-G. Redesigning the substrate specificity of ω-aminotransferase for the kinetic resolution of aliphatic chiral amines. Biotechnol Bioeng 2008;99:275–284.
83. Humble MS, Cassimjee KE, Abedi V, Federsel H-J, Berglund P. Key amino acid residues for reversed or improved enantiospecificity of an ω-transaminase. ChemCatChem 2012;4:1167–1172.
84. Clark SM, Di Leo R, Dhanoa PK, Van Cauwenberghe OR, Mullen RT, Shelp BJ. Biochemical characterization, mitochondrial localization, expression, and potential functions for an *Arabidopsis* γ-aminobutyrate transaminase that utilizes both pyruvate and glyoxylate. J Exp Bot 2009;60:1743–1757.
85. Yu H, Tang H, Wang L, Yao Y, Wu G, Xu P. Complete genome sequence of the nicotine-degrading *Pseudomonas putida* strain S16. J Bacteriol 2011;193:5541–5542.